Electronic Supplementary Material (ESI) for CrystEngComm.

Supporting Information

A series of salen-type asymmetric dinuclear Dy(III) complexes: site-resolved two-step magnetic relaxation process

Wan-Ying Zhang, Peng Chen, Yong-Mei Tian*, Hong-Feng Li, Wen-Bin Sun* and Peng-Fei Yan*

Key Laboratory of Functional Inorganic Material Chemistry Ministry of Education, School of Chemistry and Material Science Heilongjiang University, 74 Xuefu Road, Harbin 150080, P. R. China. E-mail: wenbinsun@126.com and yanpf@vip.sina.com

Table S1. Selected Bond Distances (Å) and Angles (°) for **1** and **2**.

1		**2**	
Dy1-O1	2.340(5)	Dy1-O1	2.318(4)
Dy1-O2	2.339(5)	Dy1-O2	2.325(4)
Dy1-O3	2.293(6)	Dy1-O3	2.313(5)
Dy1-O4	2.365(6)	Dy1-O4	2.342(5)
Dy1-O5	2.319(5)	Dy1-O5	2.336(5)
Dy1-O6	2.276(6)	Dy1-O6	2.297(5)
Dy1-N1	2.527(7)	Dy1-N1	2.540(6)
Dy1-N2	2.544(7)	Dy1-N2	2.546(6)
Dy1-Dy2	3.8053(8)	Dy1-Dy2	3.8586(5)
Dy2-O1	2.327(5)	Dy2-O1	2.349(4)
Dy2-O2	2.335(5)	Dy2-O2	2.368(4)
Dy2-O7	2.236(5)	Dy2-O7	2.177 (5)
Dy2-O8	2.163(6)	Dy2-O8	2.229(4)
Dy2-O9	2.385(6)	Dy2-O9	2.365(5)
Dy2-N3	2.464(6)	Dy2-N3	2.294(10)
Dy2-N4	2.477(8)	Dy2-N4	2.476(6)
O6-Dy1-O2	77.69(19)	O6-Dy1-O2	78.86(16)
O6-Dy1-O4	77.7(2)	O6-Dy1-O4	74.48(17)
O6-Dy1-O3	115.5(2)	O6-Dy1-O3	117.97(17)
O6-Dy1-O1	138.74(19)	O6-Dy1-O1	143.22(15)
O6-Dy1- N1	144.7(2)	O6-Dy1- N1	138.1(2)
O6-Dy1- N2	87.2(2)	O6-Dy1- N2	81.17(19)
O6-Dy1-O5	73.2(2)	O6-Dy1-O5	72.88(17)
O4-Dy1-N2	152.3(2)	O4-Dy1-N2	145.7(2)
O4-Dy1-N1	137.3(2)	O4-Dy1-N1	146.9(2)
O3-Dy1-O4	73.5(2)	O3-Dy1-O4	73.09(16)
O3-Dy1-O1	86.2(2)	O3-Dy1-O1	80.64(17)
O3-Dy1-O5	76.4(2)	O3-Dy1-O5	78.03(18)
O3-Dy1-N2	134.3(2)	O3-Dy1-N2	140.79(19)
O3-Dy1-N1	79.2(2)	O3-Dy1-N1	83.02(19)
O3-Dy1-O2	149.85(19)	O3-Dy1-O2	142.56(16)
O1-Dy1-O4	75.76(19)	O1-Dy1-O4	82.38(16)
O1-Dy1-O5	148.05(18)	O1-Dy1-O5	143.90(16)
O1-Dy1- N1	70.24(19)	O1-Dy1- N1	71.27(18)
O1-Dy1-N2	102.5(2)	O1-Dy1- N2	104.59(18)
O6-Dy1- N1	144.7(2)	O6-Dy1- N1	138.1(2)
O1-Dy1- O2	68.68(17)	O1-Dy1- O2	69.43(15)
O5-Dy1-O4	122.82(19)	O5-Dy1-O4	118.01(17)
O5-Dy1- N1	80.18(19)	O5-Dy1- N1	77.48(18)
O5-Dy1- N2	73.1(2)	O5-Dy1- N2	75.84(19)
N1-Dy1-N2	62.7(2)	N1-Dy1-N2	63.2(2)
O2-Dy1-O4	84.01(19)	O2-Dy1-O4	80.91(16)

O2-Dy1-O5	133.51(19)	O2-Dy1-O5	138.97(18)
O2-Dy1-N2	70.0(2)	O2-Dy1-N2	70.87(18)
O2-Dy1-N1	106.08(19)	O2-Dy1-N1	106.94(17)
O7-Dy2-O8	93.1(2)	O7-Dy2-O8	95.10(19)
O7-Dy2-O1	97.68(19)	O7-Dy2-O1	97.29(18)
O7-Dy2-N4	122.2(2)	O7-Dy2-N4	121.1(2)
O7-Dy2-N3	74.5(2)	O7-Dy2-N3	73.4(2)
O7-Dy2-O2	159.5(2)	O7-Dy2-O2	159.30(19)
O7-Dy2-O9	83.0(2)	O7-Dy2-O9	87.86(19)
O8-Dy2-O1	163.0(2)	O8-Dy2-O1	162.05(16)
O8-Dy2-N4	73.1(2)	O8-Dy2-N4	73.89(18)
O8-Dy2-N3	117.1(2)	O8-Dy2-N3	118.55(19)
O8-Dy2-O2	96.9(2)	O8-Dy2-O2	96.30(16)
O8-Dy2-O9	87.7(2)	O8-Dy2-O9	83.17(16)
O1-Dy2-N4	111.4(2)	O1-Dy2-N4	110.07(18)
O1-Dy2-N3	78.7(2)	O1-Dy2-N3	77.63(17)
O1-Dy2-O2	68.97(17)	O1-Dy2-O2	68.17(15)
O1-Dy2-O9	80.61(19)	O1-Dy2-O9	84.36(16)
N3-Dy2-N4	64.5(2)	N3-Dy2-N4	63.8(2)
O2-Dy2-N4	77.9(2)	O2-Dy2-N4	78.74(17)
O2-Dy2-N3	115.9(2)	O2-Dy2-N3	115.40(18)
O9-Dy2-N4	148.2(2)	O9-Dy2-N4	143.88(19)
O9-Dy2-N3	146.9(2)	O9-Dy2-N3	151.9(2)
O9-Dy2-O2	79.60(18)	O9-Dy2-O2	76.44(16)
Dy1-O1-Dy2	111.3(2)	Dy1-O1-Dy2	111.57(18)

Table S2. Selected Bond Distances (Å) and Angles (°) for **3**-**5**.

3		**4**		**5**	
Dy1-O1	2.348(4)	Dy1-O1	2.313(5)	Dy1-O1	2.344(3)
Dy1-O2	2.287(5)	Dy1-O2	2.312(5)	Dy1-O2	2.333(3)
Dy1-O3	2.271(5)	Dy1-O3	2.337(6)	Dy1-O3	2.357(3)
Dy1-O4	2.315(5)	Dy1-O4	2.363(6)	Dy1-O4	2.312(4)
Dy1-O5	2.277(4)	Dy1-O5	2.331(6)	Dy1-O5	2.348(4)
Dy1'-O6	2.396(11)	Dy1-O6	2.328(6)	Dy1-O6	2.269(4)
Dy1-O1'	2.316(4)	Dy1-N1	2.524(7)	Dy1-N1	2.531(4)
Dy1-N1	2.551(11)	Dy1-N2	2.470(7)	Dy1-N2	2.517(4)
Dy1-N2	2.496(12)	Dy1-Dy2	3.7524(5)	Dy1-Dy2	3.8539(3)
Dy1-Dy1'	3.8049(6)	Dy2-O1	2.297(5)	Dy2-O1	2.338(3)
Dy1'-O1	2.316(4)	Dy2-O2	2.301(5)	Dy2-O2	2.356(3)
O1-Dy1-O1'	70.68(16)	Dy2-O7	2.299(6)	Dy2-O7	2.272(4)
N2-Dy1-N1	63.2(4)	Dy2-O8	2.299(6)	Dy2-O8	2.245(4)
O1'-Dy1-N2	101.7(3)	Dy2-O9	2.312(6)	Dy2-O9	2.270(4)
O1'-Dy1-N1	67.5(3)	Dy2-O10	2.261(6)	Dy2-O10	2.256(4)
O1-Dy1-N1	106.7(3)	Dy2-O11	2.362(7)	Dy2-O11	2.443(4)
Dy1-O1-Dy1'	109.31(16)	O1-Dy1-O2	70.45(17)	O2-Dy1-O1	69.02(11)

	N1-Dy1-N2	63.5(2)	N2-Dy1-N1	62.69(14)
	O1-Dy2-O2	70.95(18)	O1-Dy2-O2	68.74(11)
	Dy2-O2-Dy1	108.8(2)	Dy2-O2-Dy1	110.55(13)
	Dy1-O1-Dy2	109.0(2)	Dy1-O1-Dy2	110.81(12)

Table S3. Dy(III) Geometry Analysis by SHAPE Software

Complex	Dy1		Dy2 (Dy1' in **3**)	
	ideal geometries	*S*	ideal geometries	*S*
1	Square antiprism (D_{4d})	0.751	Capped trigonal prism (C_{2v})	1.233
	Biaugmented trigonal prism (C_{2v})	2.095	Capped octahedron (C_{3v})	1.515
	Triangular dodecahedron (D_{2d})	2.434	Pentagonal bipyramid (D_{5h})	7.051
2	Square antiprism (D_{4d})	0.570	Capped trigonal prism (C_{2v})	1.205
	Biaugmented trigonal prism (C_{2v})	2.302	Capped octahedron (C_{3v})	2.388
	Triangular dodecahedron (D_{2d})	2.710	Pentagonal bipyramid (D_{5h})	6.186
3	Square antiprism (D_{4d})	1.127	Capped octahedron (C_{3v})	0.564
	Triangular dodecahedron (D_{2d})	1.984	Capped trigonal prism (C_{2v})	1.605
	Biaugmented trigonal prism (C_{2v})	2.534	Pentagonal bipyramid (D_{5h})	6.616
4	Square antiprism (D_{4d})	0.826	Capped octahedron (C_{3v})	0.871
	Triangular dodecahedron (D_{2d})	2.019	Capped trigonal prism (C_{2v})	1.242
	Biaugmented trigonal prism (C_{2v})	2.609	Pentagonal bipyramid (D_{5h})	6.752
5	Square antiprism (D_{4d})	1.063	Capped trigonal prism (C_{2v})	1.189
	Triangular dodecahedron (D_{2d})	1.523	Capped octahedron (C_{3v})	1.754
	Biaugmented trigonal prism (C_{2v})	2.032	Pentagonal bipyramid (D_{5h})	6.173

Table S4. Best fitted parameters (χ_T, χ_S, τ_1, α_1, τ_2, α_2 and β) with the extended Debye model for complex **2** at 1500 Oe in the temperature range 2-8.5 K.

T/K	χ_S/cm^{3}mol^{-1}	χ_T/cm^{3}mol^{-1}	τ_1/s	α_1	τ_2/s	α_2	β
2	1.50000	9.81480	0.00088	0.23000	0.02570	0.42531	0.31000
2.5	1.39998	8.67353	0.00088	0.22998	0.01988	0.44000	0.31010
3	1.25108	7.70000	0.00086	0.23000	0.01216	0.43868	0.31000
3.5	1.15002	6.70001	0.00089	0.22997	0.00654	0.43999	0.31006
4	1.05146	5.70001	0.00047	0.22997	0.00375	0.33560	0.31000
4.5	0.80002	5.30002	0.00159	0.22996	0.00097	0.44000	0.31000
5	0.80000	4.70004	0.00210	0.22973	0.00050	0.35597	0.31005
5.5	0.66648	4.40001	0.00012	0.22977	0.00107	0.29284	0.31007
6	0.63239	4.00012	0.00007	0.22941	0.00079	0.25901	0.34433
6.5	0.69747	3.59587	0.00073	0.20276	0.00009	0.32539	0.46908
7	0.37237	3.63166	0.00035	0.22997	0.00000	0.36195	0.70709
7.5	0.31428	3.42358	0.00028	0.18220	0.00000	0.39177	0.63794
8	0.31070	3.19830	0.00022	0.13001	0.00000	0.28329	0.57640
8.5	0.31978	2.98522	0.00015	0.13188	0.00000	0.34940	0.55410

Table S5. Best fitted parameters (χ_T, χ_S, τ_1, α_1, τ_2, α_2 and β) with the extended Debye model for complex **3** at 1700 Oe in the temperature range 2-8 K.

T/K	χ_S/cm^{3}mol^{-1}	χ_T/cm^{3}mol^{-1}	τ_1/s	α_1	τ_2/s	α_2	β
2	0.40000	9.20007	0.00248	0.23000	0.24574	0.44000	0.47233

2.5	0.44000	7.90028	0.00246	0.23000	0.17753	0.44000	0.56555
3	0.49997	7.00000	0.00249	0.23000	0.37095	0.43999	0.67839
3.5	0.14330	5.49363	0.00271	0.13001	0.00190	0.43998	0.31005
4	0.12153	4.90649	0.00220	0.16603	0.00089	0.43624	0.45201
4.5	0.21023	4.30862	0.00162	0.21588	0.00036	0.36471	0.63528
5	0.29998	3.81125	0.00135	0.20328	0.00030	0.29015	0.55166
5.5	0.29854	3.47126	0.00132	0.14075	0.00029	0.29843	0.31178
6	0.17403	3.30427	0.00004	0.22999	0.00059	0.22353	0.31003
6.5	0.00003	3.40470	0.00036	0.23000	0.00000	0.15149	0.69679
7	0.20152	2.80036	0.00032	0.21109	0.00001	0.24337	0.66974
7.5	0.39961	2.40794	0.00025	0.19450	0.00000	0.42541	0.70345
8	0.33562	2.30832	0.00018	0.22236	0.00000	0.43567	0.68217

Table S6. Best fitted parameters (χ_T, χ_S, τ_1, α_1, τ_2, α_2 and β) with the extended Debye model for complex **3** at 1500 Oe in the temperature range 2-8.5 K.

T/K	χ_S/cm^{3}mol^{-1}	χ_T/cm^{3}mol^{-1}	τ_1/s	α_1	τ_2/s	α_2	β
2	0.49995	12.89994	0.00962	0.23000	0.01776	0.41918	0.31002
2.5	0.25622	11.68026	0.00803	0.17460	0.00827	0.43999	0.31002
3	0.18866	9.91813	0.00638	0.20353	0.00177	0.43303	0.63599
3.5	0.41638	8.41093	0.00484	0.15573	0.00071	0.24562	0.70794
4	0.21392	7.70002	0.00326	0.13001	0.00052	0.30196	0.64898
4.5	0.32663	6.80004	0.00221	0.13000	0.00035	0.22225	0.70992
5	0.39978	6.07511	0.00155	0.13000	0.00032	0.19514	0.70996
5.5	0.39983	5.52673	0.00110	0.13000	0.00027	0.19304	0.70971
6	0.55316	4.90011	0.00082	0.13001	0.00029	0.12210	0.71000
6.5	0.23484	4.80006	0.00012	0.22999	0.00061	0.08575	0.31569
7	0.28490	4.40019	0.00015	0.19519	0.00053	0.04838	0.46879
7.5	0.30702	4.07317	0.00007	0.22107	0.00035	0.06626	0.31010
8	0.40779	3.70047	0.00006	0.20728	0.00027	0.05366	0.31019
8.5	0.29033	3.60000	0.00017	0.13017	0.00007	0.10824	0.70999

Table S7. Best fitted parameters (χ_T, χ_S, τ_1, α_1, τ_2, α_2 and β) with the extended Debye model for complex **5** at 1500 Oe in the temperature range 2-6.5 K.

T/K	χ_S/cm^{3}mol^{-1}	χ_T/cm^{3}mol^{-1}	τ_1/s	α_1	τ_2/s	α_2	β
2	4.07410	5.00010	0.00139	0.22999	0.17476	0.43999	0.55059
2.5	3.66466	5.00011	0.00128	0.23000	0.39595	0.44000	0.53503
3	3.32135	4.20011	0.00109	0.23000	0.36567	0.43999	0.60936
3.5	3.03180	3.70000	0.00090	0.23000	0.50498	0.44000	0.66618
4	2.80400	3.21667	0.00071	0.22997	0.50490	0.43997	0.70998
4.5	2.47293	4.90017	0.00068	0.29983			
5	2.11690	4.44066	0.00040	0.30000			
5.5	2.10000	4.12268	0.00034	0.30000			
6	2.05510	3.82276	0.00027	0.29929			
6.5	1.90883	3.56501	0.00020	0.30000			

Table S8. The curves are fitted by the modified Arrhenius relationship in which the QTM and Raman processes are taken account

$1/\tau = 1/\tau_{QTM} + CT^n + \tau_0^{-1}\exp(-U_{eff}/\kappa T)$

complex	q (s)	C ($s^{-1}\cdot K^{-n}$)	n	τ_0 (s)	U_{eff}/k_B (K)
3	4.4×10^{-3}	5.3×10^{-2}	2.8	1.1×10^{-5}	22.4
4	2.6×10^{-2}	4.0	3.2	2.9×10^{-6}	44.3
5	2.8×10^{-3}	12.0	3.3	9.6×10^{-4}	17.7

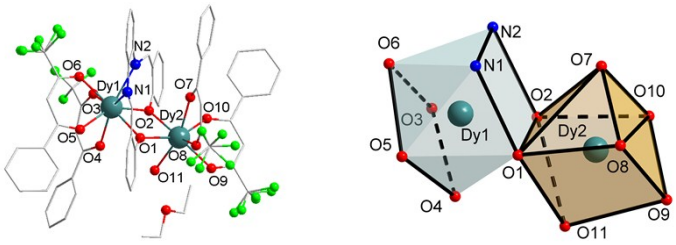

Fig. S1 The molecular structure of complex **4** (left) and local coordination geometry of the Dy(III) ions (right). Hydrogen atoms and solvent molecules are omitted for clarity.

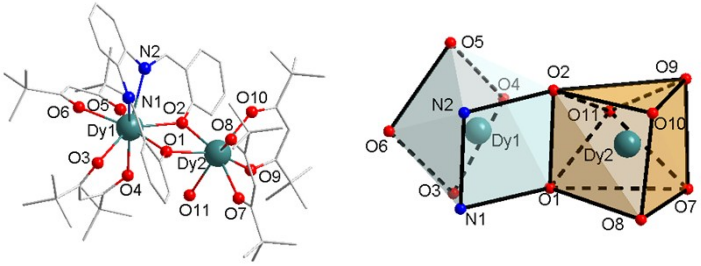

Fig. S2 The molecular structure of complex **5** (left) and local coordination geometry of the Dy(III) ions (right). Hydrogen atoms and solvent molecules are omitted for clarity.

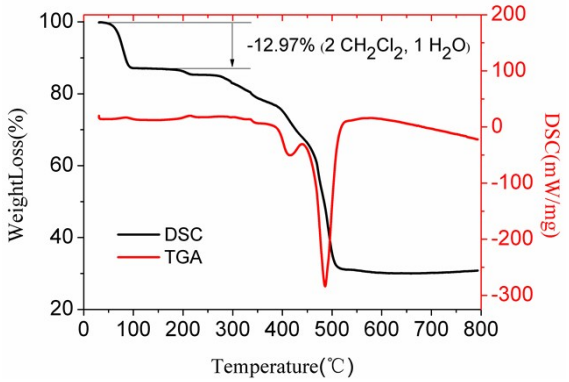

Figure S3. TG curve of compound **2**.

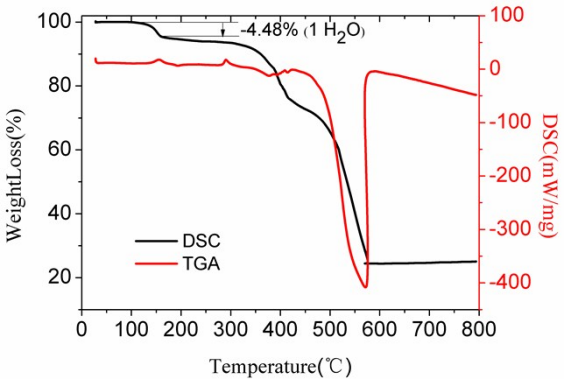

Figure S4. TG curve of compound **3**.

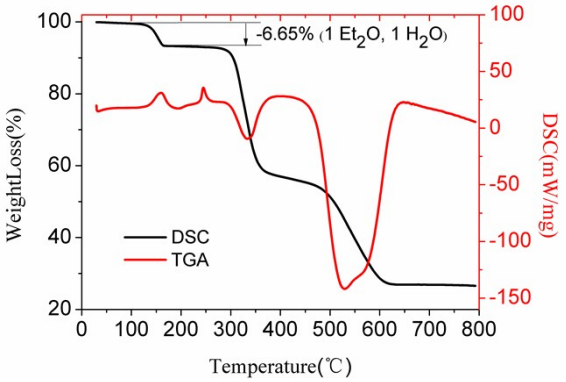

Figure S5. TG curve of compound **4**.

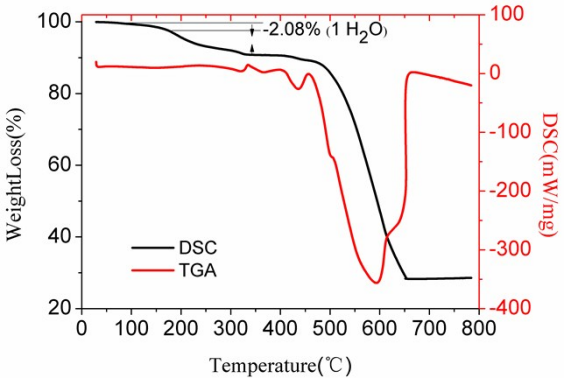

Figure S6. TG curve of compound **5**.

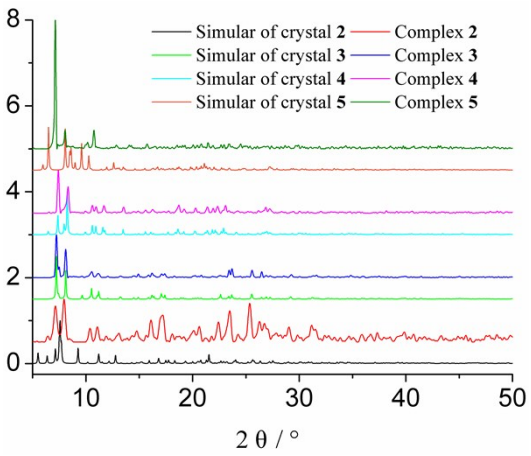

Figure S7. PXRD patterns for compounds **2**-**5**.

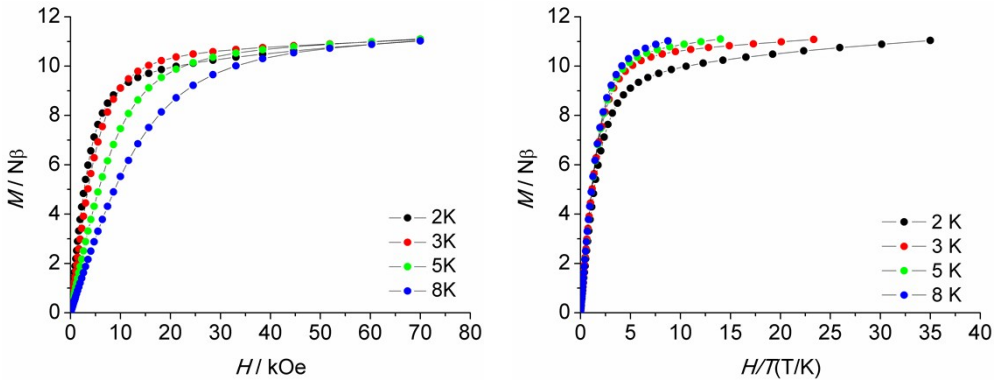

Fig. S8 The field dependence of magnetization (left) and magnetization data (right) for **2** at 2, 3, 5 and 8 K.

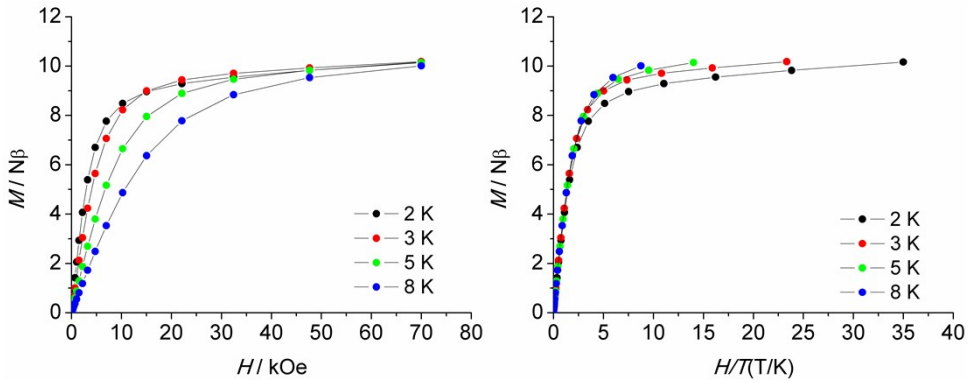

Fig. S9 The field dependence of magnetization (left) and magnetization data (right) for **3** at 2, 3, 5 and 8 K.

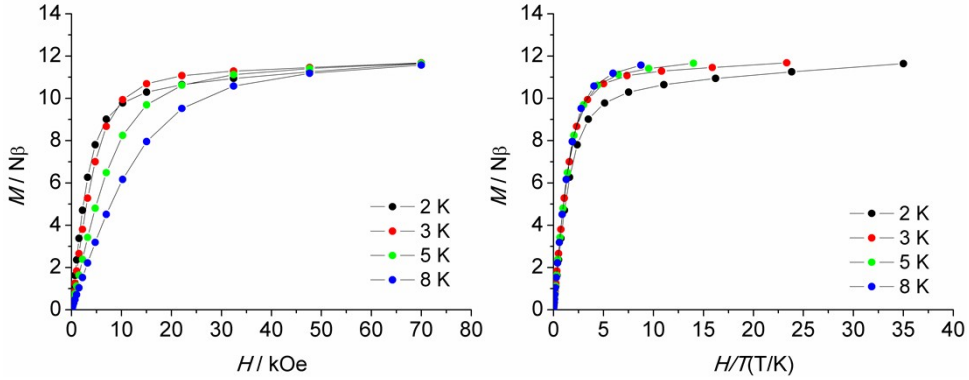

Fig. S10 The field dependence of magnetization (left) and magnetization data (right) for **4** at 2, 3, 5 and 8 K.

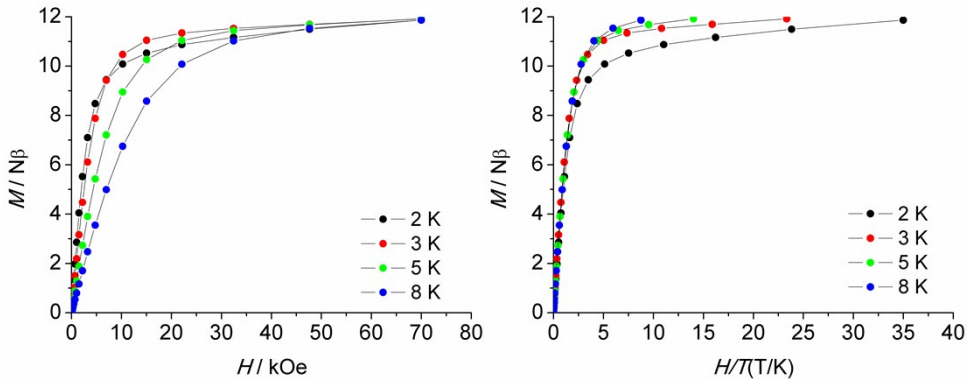

Fig. S11 The field dependence of magnetization (left) and magnetization data (right) for **5** at 2, 3, 5 and 8 K.

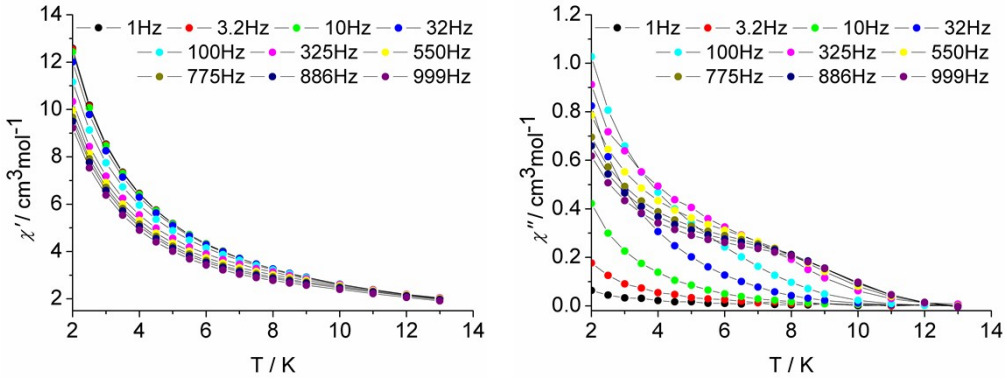

Fig. S12 Plots of the temperature dependent in-phase (χ') and out-of-phase ac susceptibility (χ'') under 0 Oe field for **2**.

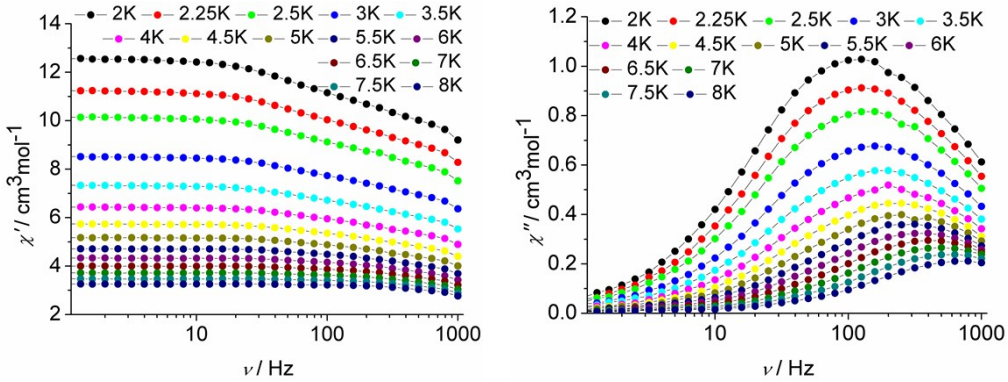

Fig. S13 Plots of the frequency dependent in-phase (χ') and out-of-phase ac susceptibility (χ'') under 0 Oe field for **2**.

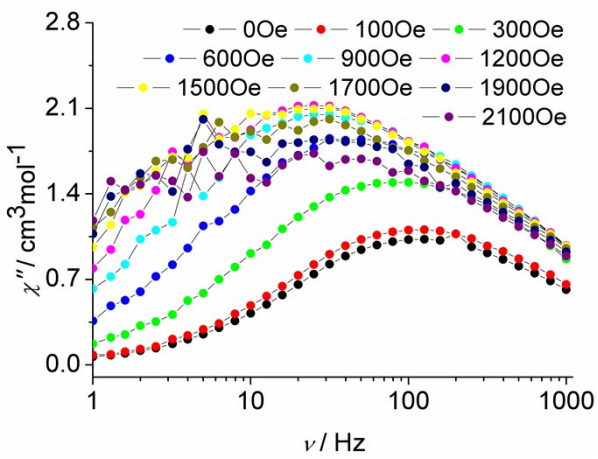

Fig. S14 Plot of the frequency dependence of the out-of-phase (χ'') ac susceptibility component under indicated dc field at 2 K for complex **2**.

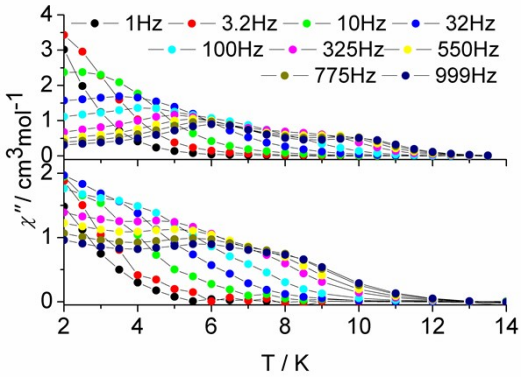

Fig. S15 Temperature dependence of the out-of-phase (*χ''*) ac susceptibility of complex **1** (top) and complex **2** (bottom) in the frequency range 1-1000 Hz under 1500 Oe.

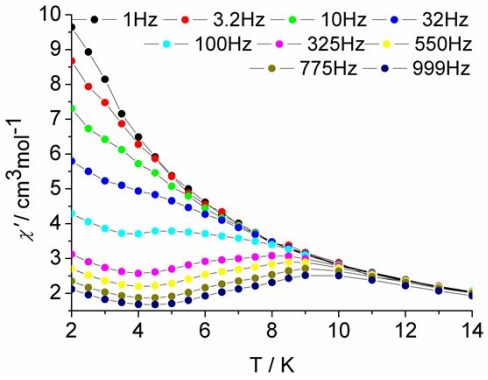

Fig. S16 Temperature dependence of the in-phase (χ') ac susceptibility in the frequency range 1-1000 Hz of complex **2** under 1500 Oe.

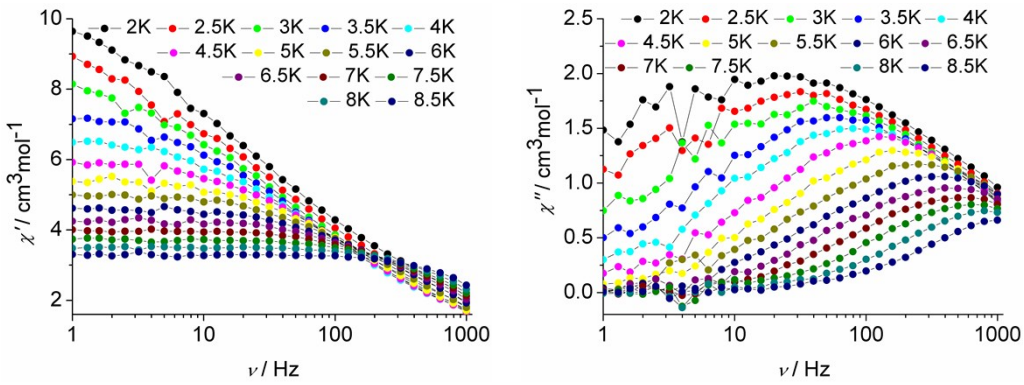

Fig. S17 Plots of the frequency dependent in-phase (χ') and out-of-phase ac susceptibility (χ'') under 1500 Oe field for **2**.

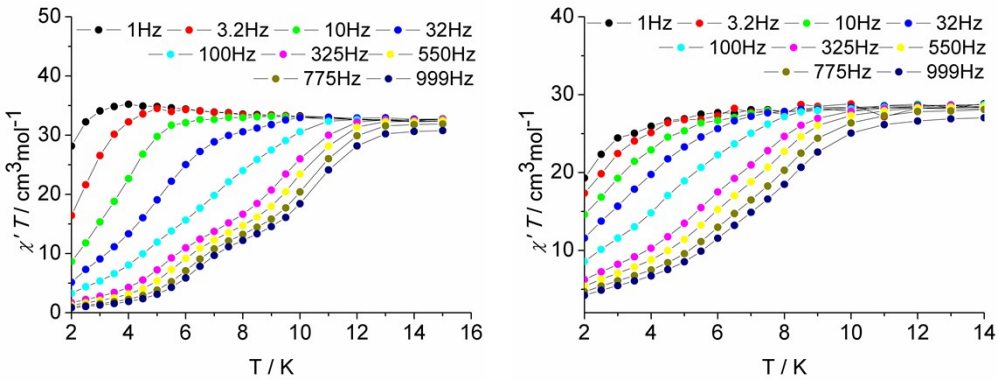

Fig. S18 Temperature dependence of the out-of-phase $\chi'T$ ac susceptibility of complex **1** (left) and complex **2** (right) in the frequency range 1-1000 Hz under the optimum fields.

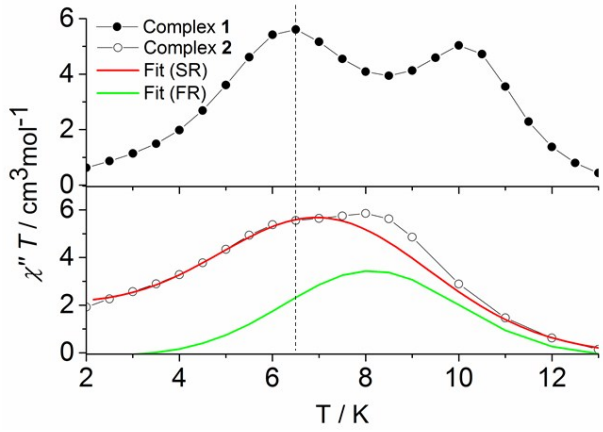

Fig. S19 Comparison of temperature dependence of the out-of-phase (χ'') ac susceptibility for complex **1** and complex **2** at 999 Hz under 1500 Oe. Fitting of the peak position to determine the individual relaxation time. The dashed lines indicate the consistent low-temperature relaxation process of the two complexes.

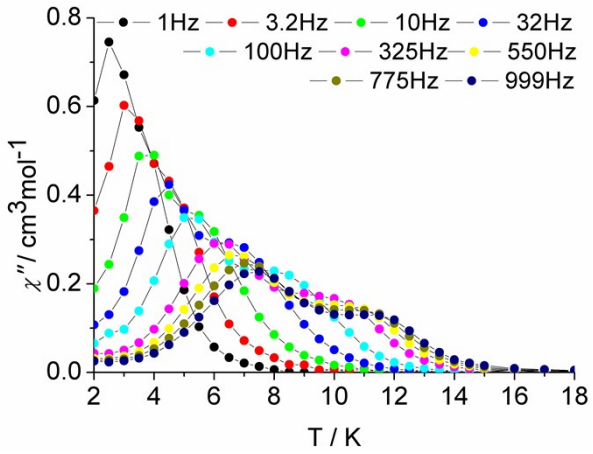

Fig. S20 Temperature dependence of the out-of-phase (χ'') ac susceptibility of **1a** in the frequency range 1-1000 Hz under 1500 Oe.

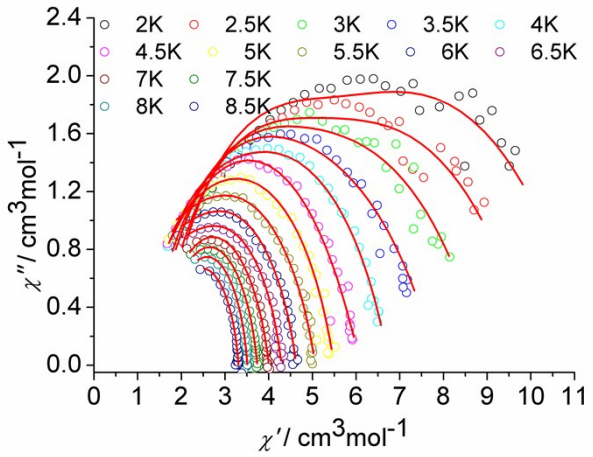

Fig. S21 Cole-Cole plot for complex **2** obtained using the ac susceptibility data under 1500 Oe. The solid lines correspond to the best fit obtained with the sum of two modified Debye functions.

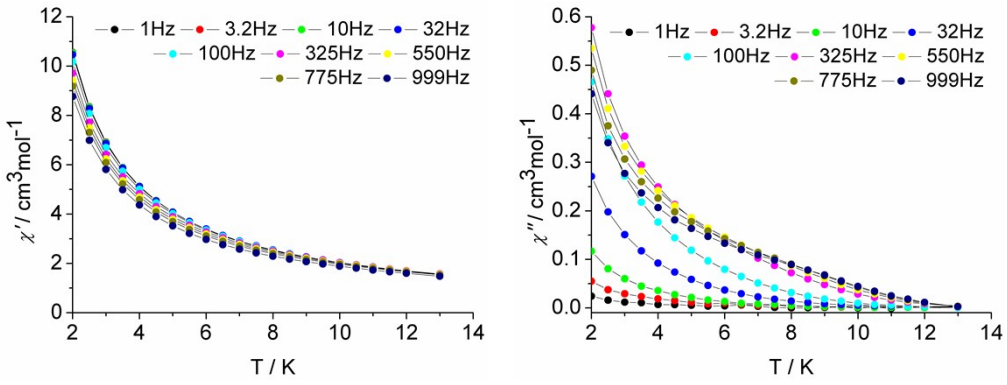

Fig. S22 Plots of the temperature dependent in-phase (χ') and out-of-phase ac susceptibility (χ'') under 0 Oe field for **3**.

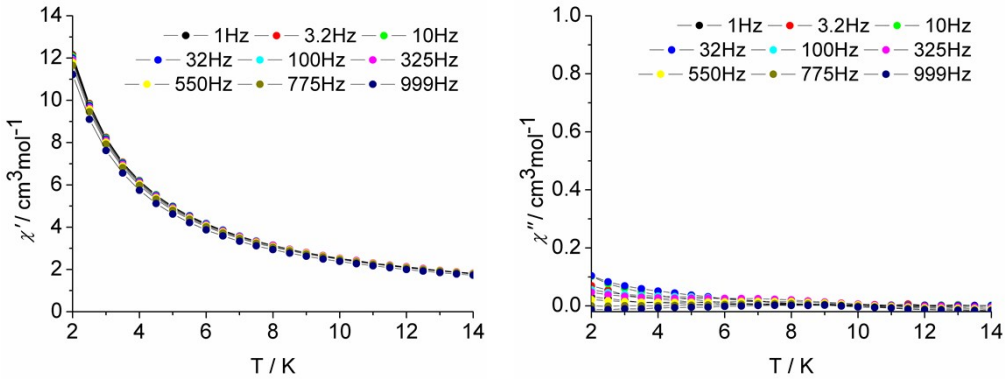

Fig. S23 Plots of the temperature dependent in-phase (χ') and out-of-phase ac susceptibility (χ'') under 0 Oe field for **4**.

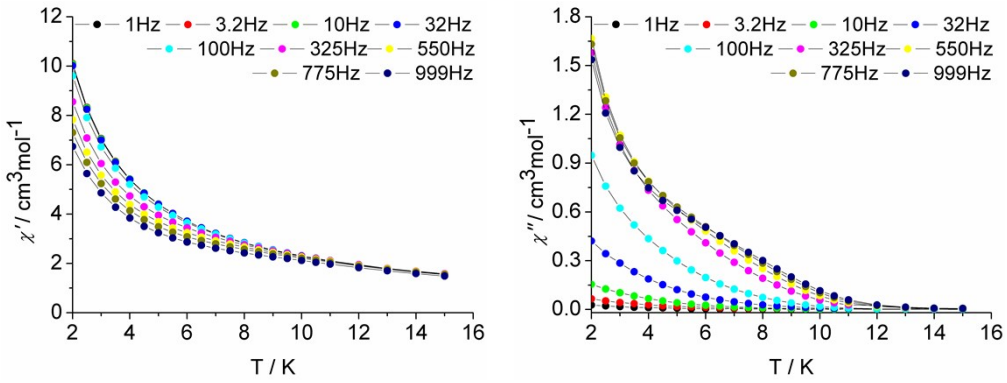

Fig. S24 Plots of the temperature dependent in-phase (χ') and out-of-phase ac susceptibility (χ'') under 0 Oe field for **5**.

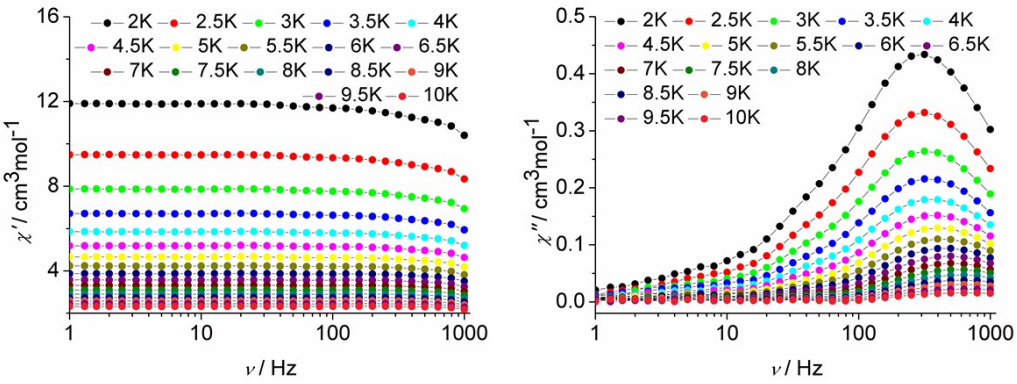

Fig. S25 Plots of the frequency dependent in-phase (χ') and out-of-phase ac susceptibility (χ'') under 0 Oe field for **3**.

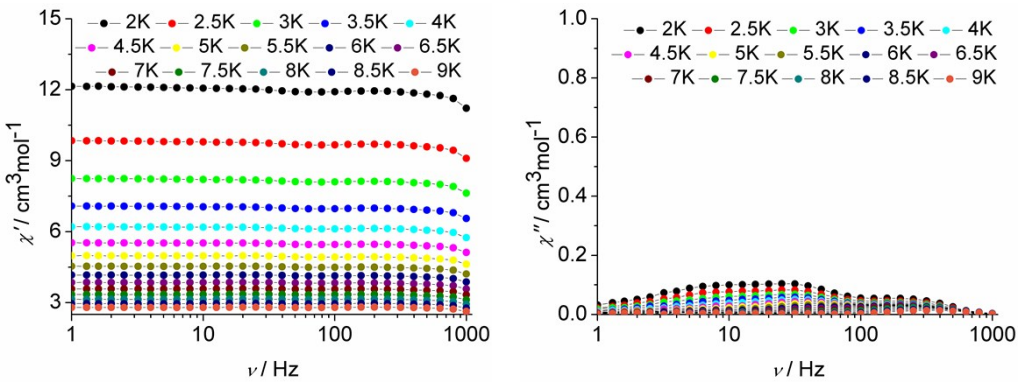

Fig. S26 Plots of the frequency dependent in-phase (χ') and out-of-phase ac susceptibility (χ'') under 0 Oe field for **4**.

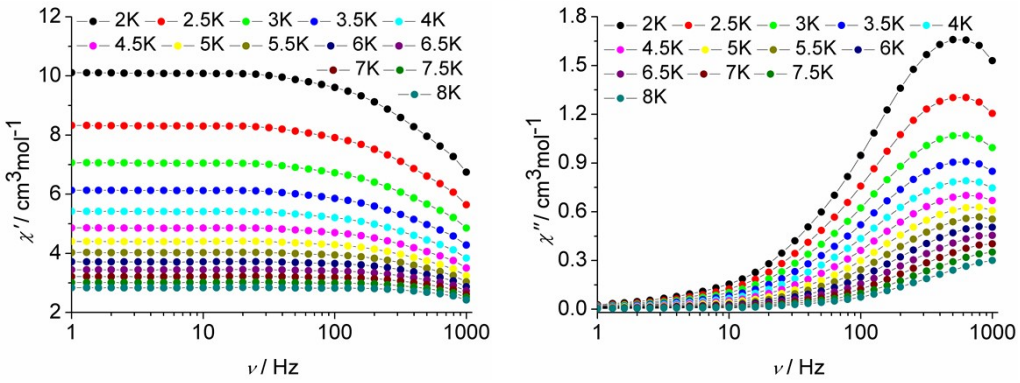

Fig. S27 Plots of the frequency dependent in-phase (χ') and out-of-phase ac susceptibility (χ'') under 0 Oe field for **5**.

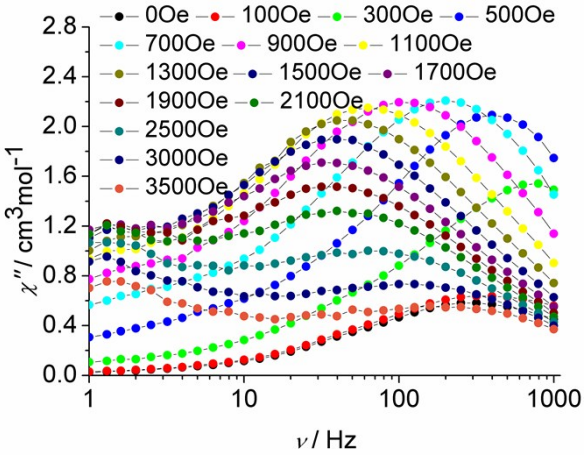

Fig. S28 Plot of the frequency dependence of the out-of-phase (χ'') ac susceptibility component under indicated dc field at 2 K for complex **3**.

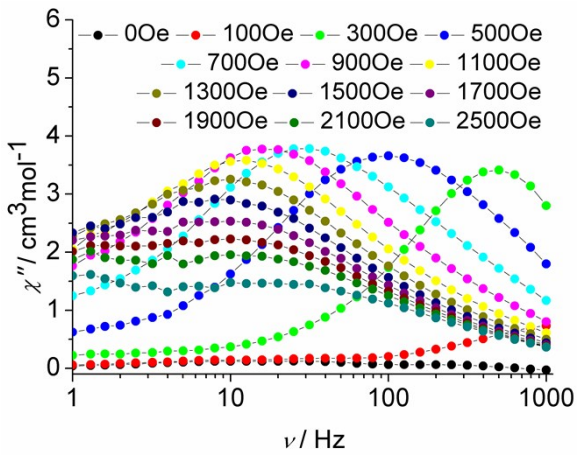

Fig. S29 Plot of the frequency dependence of the out-of-phase (χ'') ac susceptibility component under indicated dc field at 2 K for complex **4**.

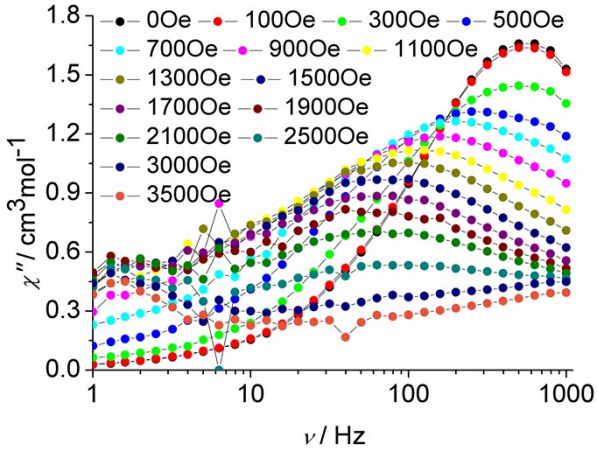

Fig. S30 Plot of the frequency dependence of the out-of-phase (χ'') ac susceptibility component under indicated dc field at 2 K for complex **5**.

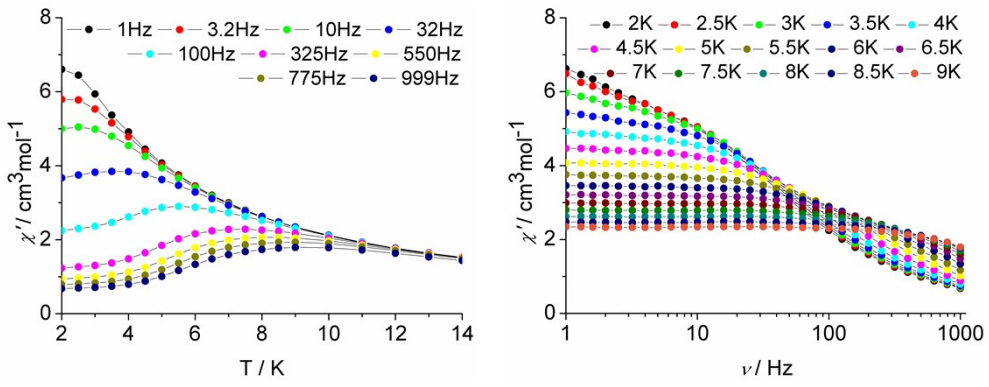

Fig. S31 Temperature dependence of the in-phase (χ') ac susceptibility (left) and frequency dependence of the in-phase (χ') ac susceptibility (right) of complex **3** under 1700 Oe.

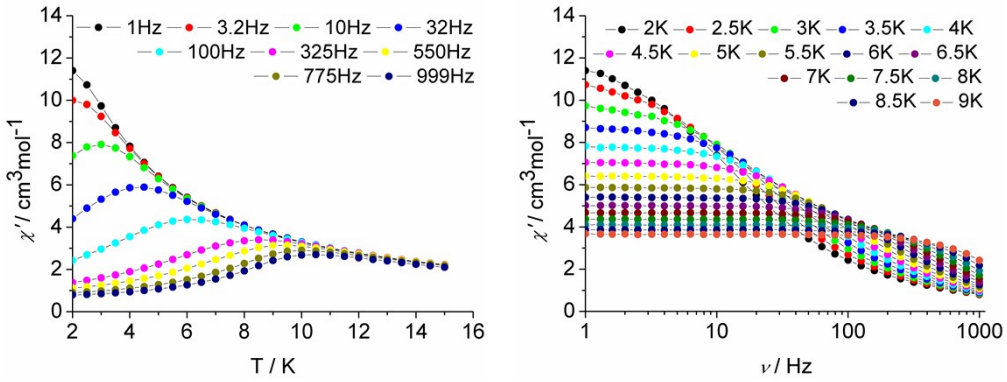

Fig. S32 Temperature dependence of the in-phase (χ') ac susceptibility (left) and frequency dependence of the in-phase (χ') ac susceptibility (right) of complex **4** under 1500 Oe.

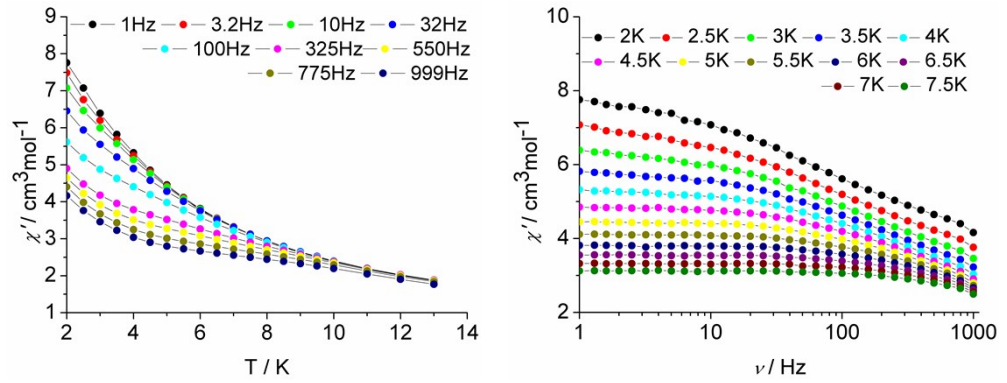

Fig. S33 Temperature dependence of the in-phase (χ') ac susceptibility (left) and frequency dependence of the in-phase (χ') ac susceptibility (right) of complex **5** under 1500 Oe.

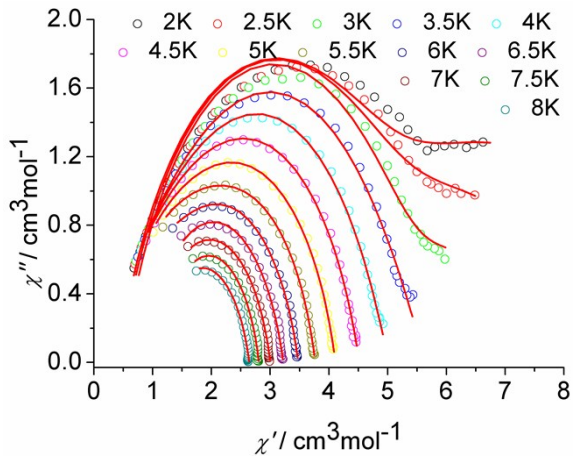

Fig. S34 Cole-Cole plot for complex **3** obtained using the ac susceptibility data under 1700 Oe. The solid lines correspond to the best fit obtained with the sum of two modified Debye functions.

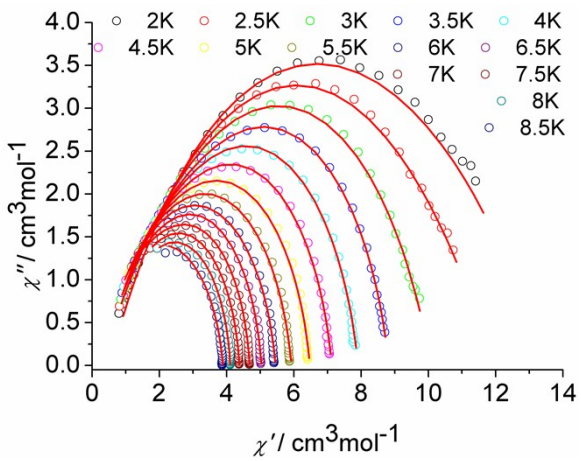

Fig. S35 Cole-Cole plot for complex **4** obtained using the ac susceptibility data under 1500 Oe. The solid lines correspond to the best fit obtained with the sum of two modified Debye functions.

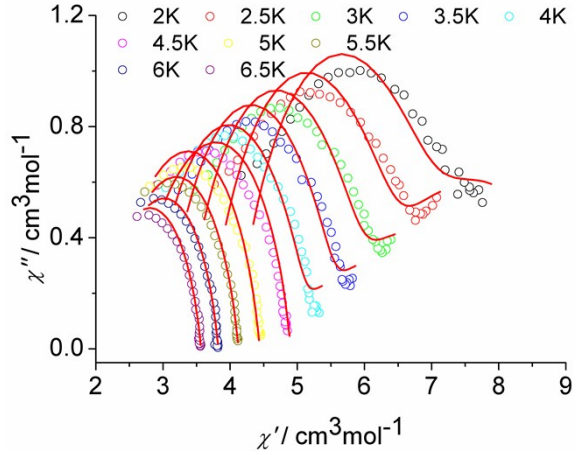

Fig. S36 Cole-Cole plot for complex **5** obtained using the ac susceptibility data under 1500 Oe. The solid lines correspond to the best fit obtained with the sum of two modified Debye functions.

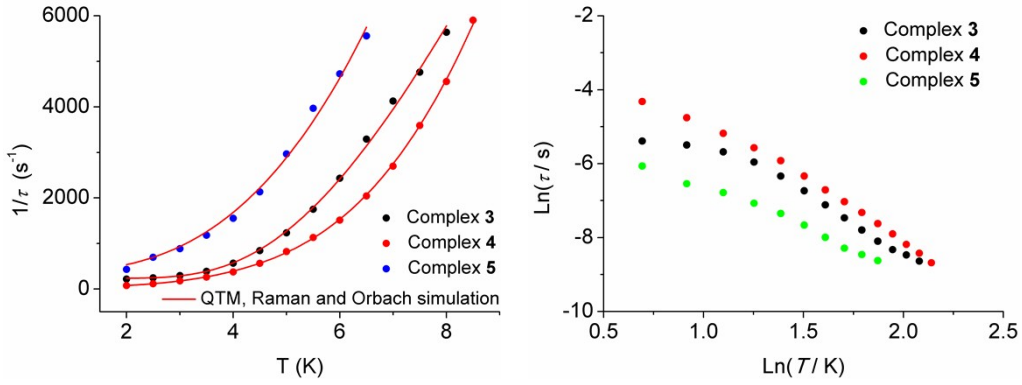

Fig. S37 Temperature dependence of the inverse relaxation time $1/\tau$ (left) and temperature dependency of relaxation time in a log-log scale $\ln\tau$ vs $\ln T$ (right) under the optimum fields for **3**-**5**. The red lines represent the fitting of the frequency-dependent data by Equation 1 for **3**-**5**.

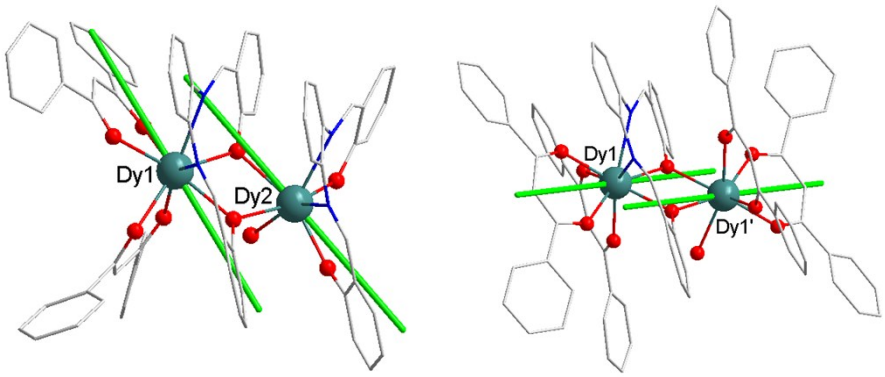

Fig. S38 Orientations of the anisotropy axes for each of the two Dy(III) ions in complexes **2** (left) and **3** (right) as calculated by MAGELLAN.